Measurements of the center-of-mass energies at BESIII via the di-muon process

M. Ablikim[1], M. N. Achasov[9,f], X. C. Ai[1], O. Albayrak[5], M. Albrecht[4], D. J. Ambrose[44], A. Amoroso[49A,49C], F. F. An[1], Q. An[46,a], J. Z. Bai[1], R. Baldini Ferroli[20A], Y. Ban[31], D. W. Bennett[19], J. V. Bennett[5], M. Bertani[20A], D. Bettoni[21A], J. M. Bian[43], F. Bianchi[49A,49C], E. Boger[23,d], I. Boyko[23], R. A. Briere[5], H. Cai[51], X. Cai[1,a], O. Cakir[40A,b], A. Calcaterra[20A], G. F. Cao[1], S. A. Cetin[40B], J. F. Chang[1,a], G. Chelkov[23,d,e], G. Chen[1], H. S. Chen[1], H. Y. Chen[2], J. C. Chen[1], M. L. Chen[1,a], S. J. Chen[29], X. Chen[1,a], X. R. Chen[26], Y. B. Chen[1,a], H. P. Cheng[17], X. K. Chu[31], G. Cibinetto[21A], H. L. Dai[1,a], J. P. Dai[34], A. Dbeyssi[14], D. Dedovich[23], Z. Y. Deng[1], A. Denig[22], I. Denysenko[23], M. Destefanis[49A,49C], F. De Mori[49A,49C], Y. Ding[27], C. Dong[30], J. Dong[1,a], L. Y. Dong[1], M. Y. Dong[1,a], S. X. Du[53], P. F. Duan[1], J. Z. Fan[39], J. Fang[1,a], S. S. Fang[1], X. Fang[46,a], Y. Fang[1], L. Fava[49B,49C], F. Feldbauer[22], G. Felici[20A], C. Q. Feng[46,a], E. Fioravanti[21A], M. Fritsch[14,22], C. D. Fu[1], Q. Gao[1], X. L. Gao[46,a], X. Y. Gao[2], Y. Gao[39], Z. Gao[46,a], I. Garzia[21A], K. Goetzen[10], W. X. Gong[1,a], W. Gradl[22], M. Greco[49A,49C], M. H. Gu[1,a], Y. T. Gu[12], Y. H. Guan[1], A. Q. Guo[1], L. B. Guo[28], Y. Guo[1], Y. P. Guo[22], Z. Haddadi[25], A. Hafner[22], S. Han[51], X. Q. Hao[15], F. A. Harris[42], K. L. He[1], X. Q. He[45], T. Held[4], Y. K. Heng[1,a], Z. L. Hou[1], C. Hu[28], H. M. Hu[1], J. F. Hu[49A,49C], T. Hu[1,a], Y. Hu[1], G. M. Huang[6], G. S. Huang[46,a], J. S. Huang[15], X. T. Huang[33], Y. Huang[29], T. Hussain[48], Q. Ji[1], Q. P. Ji[30], X. B. Ji[1], X. L. Ji[1,a], L. W. Jiang[51], X. S. Jiang[1,a], X. Y. Jiang[30], J. B. Jiao[33], Z. Jiao[17], D. P. Jin[1,a], S. Jin[1], T. Johansson[50], A. Julin[43], N. Kalantar-Nayestanaki[25], X. L. Kang[1], X. S. Kang[30], M. Kavatsyuk[25], B. C. Ke[5], P. Kiese[22], R. Kliemt[14], B. Kloss[22], O. B. Kolcu[40B,i], B. Kopf[4], M. Kornicer[42], W. Kühn[24], A. Kupsc[50], J. S. Lange[24], M. Lara[19], P. Larin[14], C. Leng[49C], C. Li[50], Cheng Li[46,a], D. M. Li[53], F. Li[1,a], F. Y. Li[31], G. Li[1], H. B. Li[1], J. C. Li[1], Jin Li[32], K. Li[13], K. Li[33], Lei Li[3], P. R. Li[41], T. Li[33], W. D. Li[1], W. G. Li[1], X. L. Li[33], X. M. Li[12], X. N. Li[1,a], X. Q. Li[30], Z. B. Li[38], H. Liang[46,a], Y. F. Liang[36], Y. T. Liang[24], G. R. Liao[11], D. X. Lin[14], B. J. Liu[1], C. X. Liu[1], D. Liu[46,a], F. H. Liu[35], Fang Liu[1], Feng Liu[6], H. B. Liu[12], H. H. Liu[1], H. H. Liu[16], H. M. Liu[1], J. Liu[1], J. B. Liu[46,a], J. P. Liu[51], J. Y. Liu[1], K. Liu[39], K. Y. Liu[27], L. D. Liu[31], P. L. Liu[1,a], Q. Liu[41], S. B. Liu[46,a], X. Liu[26], Y. B. Liu[30], Z. A. Liu[1,a], Zhiqing Liu[22], H. Loehner[25], X. C. Lou[1,a,h], H. J. Lu[17], J. G. Lu[1,a], Y. Lu[1], Y. P. Lu[1,a], C. L. Luo[28], M. X. Luo[52], T. Luo[42], X. L. Luo[1,a], X. R. Lyu[41], F. C. Ma[27], H. L. Ma[1], L. L. Ma[33], Q. M. Ma[1], T. Ma[1], X. N. Ma[30], X. Y. Ma[1,a], F. E. Maas[14], M. Maggiora[49A,49C], Y. J. Mao[31], Z. P. Mao[1], S. Marcello[49A,49C], J. G. Messchendorp[25], J. Min[1,a], R. E. Mitchell[19], X. H. Mo[1,a], Y. J. Mo[6], C. Morales Morales[14], K. Moriya[19], N. Yu. Muchnoi[9,f], H. Muramatsu[43], Y. Nefedov[23], F. Nerling[14], I. B. Nikolaev[9,f], Z. Ning[1,a], S. Nisar[8], S. L. Niu[1,a], X. Y. Niu[1], S. L. Olsen[32], Q. Ouyang[1,a], S. Pacetti[20B], Y. Pan[46,a], P. Patteri[20A], M. Pelizaeus[4], H. P. Peng[46,a], K. Peters[10], J. Pettersson[50], J. L. Ping[28], R. G. Ping[1], R. Poling[43], V. Prasad[1], M. Qi[29], S. Qian[1,a], C. F. Qiao[41], L. Q. Qin[33], N. Qin[51], X. S. Qin[1], Z. H. Qin[1,a], J. F. Qiu[1], K. H. Rashid[48], C. F. Redmer[22], M. Ripka[22], G. Rong[1], Ch. Rosner[14], X. D. Ruan[12], V. Santoro[21A], A. Sarantsev[23,g], M. Savrié[21B], K. Schoenning[50], S. Schumann[22], W. Shan[31], M. Shao[46,a], C. P. Shen[2], P. X. Shen[30], X. Y. Shen[1], H. Y. Sheng[1], W. M. Song[1], X. Y. Song[1], S. Sosio[49A,49C], S. Spataro[49A,49C], G. X. Sun[1], J. F. Sun[15], S. S. Sun[1], Y. J. Sun[46,a], Y. Z. Sun[1], Z. J. Sun[1,a], Z. T. Sun[19], C. J. Tang[36], X. Tang[1], I. Tapan[40C], E. H. Thorndike[44], M. Tiemens[25], M. Ullrich[24], I. Uman[40B], G. S. Varner[42], B. Wang[30], D. Wang[31], D. Y. Wang[31], K. Wang[1,a], L. L. Wang[1], L. S. Wang[1], M. Wang[33], P. Wang[1], P. L. Wang[1], S. G. Wang[31], W. Wang[1,a], W. P. Wang[46,a], X. F. Wang[39], Y. D. Wang[14], Y. F. Wang[1,a], Y. Q. Wang[22], Z. Wang[1,a], Z. G. Wang[1,a], Z. H. Wang[46,a], Z. Y. Wang[1], T. Weber[22], D. H. Wei[11], J. B. Wei[31], P. Weidenkaff[22], S. P. Wen[1], U. Wiedner[4], M. Wolke[50], L. H. Wu[1], Z. Wu[1,a], L. Xia[46,a], L. G. Xia[39], Y. Xia[18], D. Xiao[1], H. Xiao[47], Z. J. Xiao[28], Y. G. Xie[1,a], Q. L. Xiu[1,a], G. F. Xu[1], L. Xu[1], Q. J. Xu[13], X. P. Xu[37], L. Yan[49A,49C], W. B. Yan[46,a], W. C. Yan[46,a], Y. H. Yan[18], H. J. Yang[34], H. X. Yang[1], L. Yang[51], Y. Yang[6], Y. X. Yang[11], M. Ye[1,a], M. H. Ye[7], J. H. Yin[1], B. X. Yu[1,a], C. X. Yu[30], J. S. Yu[26], C. Z. Yuan[1], W. L. Yuan[29], Y. Yuan[1], A. Yuncu[40B,c], A. A. Zafar[48], A. Zallo[20A], Y. Zeng[18], Z. Zeng[46,a], B. X. Zhang[1], B. Y. Zhang[1,a], C. Zhang[29], C. C. Zhang[1], D. H. Zhang[1], H. H. Zhang[38], H. Y. Zhang[1,a], J. J. Zhang[1], J. L. Zhang[1], J. Q. Zhang[1], J. W. Zhang[1,a], J. Y. Zhang[1], J. Z. Zhang[1], K. Zhang[1], L. Zhang[1], X. Y. Zhang[33], Y. Zhang[1], Y. N. Zhang[41], Y. H. Zhang[1,a], Y. T. Zhang[46,a], Yu Zhang[41], Z. H. Zhang[6], Z. P. Zhang[46], Z. Y. Zhang[51], G. Zhao[1], J. W. Zhao[1,a], J. Y. Zhao[1], J. Z. Zhao[1,a], Lei Zhao[46,a], Ling Zhao[1], M. G. Zhao[30], Q. Zhao[1], Q. W. Zhao[1], S. J. Zhao[53], T. C. Zhao[1], Y. B. Zhao[1,a], Z. G. Zhao[46,a], A. Zhemchugov[23,d], B. Zheng[47], J. P. Zheng[1,a], W. J. Zheng[33], Y. H. Zheng[41], B. Zhong[28], L. Zhou[1,a], X. Zhou[51], X. K. Zhou[46,a], X. R. Zhou[46,a], X. Y. Zhou[1], K. Zhu[1], K. J. Zhu[1,a], S. Zhu[1], S. H. Zhu[45], X. L. Zhu[39], Y. C. Zhu[46,a], Y. S. Zhu[1], Z. A. Zhu[1], J. Zhuang[1,a], L. Zotti[49A,49C], B. S. Zou[1], J. H. Zou[1]

(BESIII Collaboration)

[1] *Institute of High Energy Physics, Beijing 100049, People's Republic of China*
[2] *Beihang University, Beijing 100191, People's Republic of China*
[3] *Beijing Institute of Petrochemical Technology, Beijing 102617, People's Republic of China*
[4] *Bochum Ruhr-University, D-44780 Bochum, Germany*
[5] *Carnegie Mellon University, Pittsburgh, Pennsylvania 15213, USA*
[6] *Central China Normal University, Wuhan 430079, People's Republic of China*
[7] *China Center of Advanced Science and Technology, Beijing 100190, People's Republic of China*
[8] *COMSATS Institute of Information Technology, Lahore, Defence Road, Off Raiwind Road, 54000 Lahore, Pakistan*
[9] *G.I. Budker Institute of Nuclear Physics SB RAS (BINP), Novosibirsk 630090, Russia*
[10] *GSI Helmholtzcentre for Heavy Ion Research GmbH, D-64291 Darmstadt, Germany*
[11] *Guangxi Normal University, Guilin 541004, People's Republic of China*
[12] *GuangXi University, Nanning 530004, People's Republic of China*
[13] *Hangzhou Normal University, Hangzhou 310036, People's Republic of China*
[14] *Helmholtz Institute Mainz, Johann-Joachim-Becher-Weg 45, D-55099 Mainz, Germany*
[15] *Henan Normal University, Xinxiang 453007, People's Republic of China*
[16] *Henan University of Science and Technology, Luoyang 471003, People's Republic of China*
[17] *Huangshan College, Huangshan 245000, People's Republic of China*
[18] *Hunan University, Changsha 410082, People's Republic of China*

[19] *Indiana University, Bloomington, Indiana 47405, USA*
[20] *(A)INFN Laboratori Nazionali di Frascati, I-00044, Frascati, Italy; (B)INFN and University of Perugia, I-06100, Perugia, Italy*
[21] *(A)INFN Sezione di Ferrara, I-44122, Ferrara, Italy; (B)University of Ferrara, I-44122, Ferrara, Italy*
[22] *Johannes Gutenberg University of Mainz, Johann-Joachim-Becher-Weg 45, D-55099 Mainz, Germany*
[23] *Joint Institute for Nuclear Research, 141980 Dubna, Moscow region, Russia*
[24] *Justus Liebig University Giessen, II. Physikalisches Institut, Heinrich-Buff-Ring 16, D-35392 Giessen, Germany*
[25] *KVI-CART, University of Groningen, NL-9747 AA Groningen, The Netherlands*
[26] *Lanzhou University, Lanzhou 730000, People's Republic of China*
[27] *Liaoning University, Shenyang 110036, People's Republic of China*
[28] *Nanjing Normal University, Nanjing 210023, People's Republic of China*
[29] *Nanjing University, Nanjing 210093, People's Republic of China*
[30] *Nankai University, Tianjin 300071, People's Republic of China*
[31] *Peking University, Beijing 100871, People's Republic of China*
[32] *Seoul National University, Seoul, 151-747 Korea*
[33] *Shandong University, Jinan 250100, People's Republic of China*
[34] *Shanghai Jiao Tong University, Shanghai 200240, People's Republic of China*
[35] *Shanxi University, Taiyuan 030006, People's Republic of China*
[36] *Sichuan University, Chengdu 610064, People's Republic of China*
[37] *Soochow University, Suzhou 215006, People's Republic of China*
[38] *Sun Yat-Sen University, Guangzhou 510275, People's Republic of China*
[39] *Tsinghua University, Beijing 100084, People's Republic of China*
[40] *(A)Istanbul Aydin University, 34295 Sefakoy, Istanbul, Turkey; (B)Dogus University, 34722 Istanbul, Turkey; (C)Uludag University, 16059 Bursa, Turkey*
[41] *University of Chinese Academy of Sciences, Beijing 100049, People's Republic of China*
[42] *University of Hawaii, Honolulu, Hawaii 96822, USA*
[43] *University of Minnesota, Minneapolis, Minnesota 55455, USA*
[44] *University of Rochester, Rochester, New York 14627, USA*
[45] *University of Science and Technology Liaoning, Anshan 114051, People's Republic of China*
[46] *University of Science and Technology of China, Hefei 230026, People's Republic of China*
[47] *University of South China, Hengyang 421001, People's Republic of China*
[48] *University of the Punjab, Lahore-54590, Pakistan*
[49] *(A)University of Turin, I-10125, Turin, Italy; (B)University of Eastern Piedmont, I-15121, Alessandria, Italy; (C)INFN, I-10125, Turin, Italy*
[50] *Uppsala University, Box 516, SE-75120 Uppsala, Sweden*
[51] *Wuhan University, Wuhan 430072, People's Republic of China*
[52] *Zhejiang University, Hangzhou 310027, People's Republic of China*
[53] *Zhengzhou University, Zhengzhou 450001, People's Republic of China*

[a] *Also at State Key Laboratory of Particle Detection and Electronics, Beijing 100049, Hefei 230026, People's Republic of China*
[b] *Also at Ankara University,06100 Tandogan, Ankara, Turkey*
[c] *Also at Bogazici University, 34342 Istanbul, Turkey*
[d] *Also at the Moscow Institute of Physics and Technology, Moscow 141700, Russia*
[e] *Also at the Functional Electronics Laboratory, Tomsk State University, Tomsk, 634050, Russia*
[f] *Also at the Novosibirsk State University, Novosibirsk, 630090, Russia*
[g] *Also at the NRC "Kurchatov Institute", PNPI, 188300, Gatchina, Russia*
[h] *Also at University of Texas at Dallas, Richardson, Texas 75083, USA*
[i] *Also at Istanbul Arel University, 34295 Istanbul, Turkey*

From 2011 to 2014, the BESIII experiment collected about 5 fb^{-1} data at center-of-mass energies around 4 GeV for the studies of the charmonium-like and higher excited charmonium states. By analyzing the di-muon process $e^+e^- \to \gamma_{\rm ISR/FSR}\mu^+\mu^-$, the center-of-mass energies of the data samples are measured with a precision of 0.8 MeV. The center-of-mass energy is found to be stable for most of time during the data taking.

PACS numbers: 06.30.-k, 13.66.Jn

I. INTRODUCTION

The BESIII detector operating at the BEPCII accelerator is designed to study physics in the τ-charm energy region (2$\sim$4.6 GeV) [1]. From 2011 to 2014, the BESIII experiment accumulated 5 fb^{-1} of e^+e^- collision data at center-of-mass energies between 3.810 and 4.600 GeV to study the charmonium-like and higher excited charmonium states [2]. In the past, BESIII has taken large data samples at the J/ψ, $\psi(3686)$ and $\psi(3770)$ peaks. The corresponding beam energy was fine tuned by a J/ψ or $\psi(3686)$ mass scan before the data-taking. However, around 4 GeV, there is no narrow resonance in e^+e^- annihilation, and the $\psi(3686)$ peak is too far away to be used to calibrate the beam energy. The Beam Energy Measurement System (BEMS), which was installed in 2008, is designed to measure the beam energy with a relative

systematic uncertainty of 2×10^{-5} [3] based on the energies of Compton back-scattered photons. The performance of the BEMS is verified through the measurement of the $\psi(3686)$ mass, but 4 GeV is beyond the working range of BEMS. To precisely measure the masses of the newly observed Z_c [4, 5] particles, especially for those which are observed by a partial reconstruction method [6, 7], a precise knowledge of the center-of-mass energy ($E_{\rm cms}$) is crucial.

In this paper, we develop a method to measure the $E_{\rm cms}$ using the di-muon process

$$e^+e^- \to \gamma_{\rm ISR/FSR}\mu^+\mu^-, \quad (1)$$

where $\gamma_{\rm ISR/FSR}$ represents possible initial state radiative (ISR) or final state radiative (FSR) photons. The $E_{\rm cms}$ can be written as

$$E_{\rm cms} = M(\mu^+\mu^-) + \Delta M_{\rm ISR/FSR}, \quad (2)$$

where $M(\mu^+\mu^-)$ is the invariant mass of $\mu^+\mu^-$, $\Delta M_{\rm ISR/FSR}$ is the mass shift due to ISR/FSR radiation, which equals to the difference between the invariant mass of the $\mu^+\mu^-$ pair and the $E_{\rm cms}$ of the initial e^+e^- system. In the analysis, $\Delta M_{\rm ISR/FSR}$ is estimated from a Monte Carlo (MC) simulation of the di-muon process by turning on or off the ISR/FSR, where the ISR/FSR is simulated by BABAYAGA3.5 [9]. To make sure the measured invariant mass $M(\mu^+\mu^-)$ is unbiased, we validate the reconstructed momentum of μ^+/μ^- with the J/ψ signal from the process $e^+e^- \to \gamma_{\rm ISR}J/\psi$ with $J/\psi \to \mu^+\mu^-(\gamma_{\rm FSR})$ in the same data samples.

II. THE BESIII DETECTOR AND DATA SETS

The BESIII detector is described in detail in Ref. [10]. The detector is cylindrically symmetric and covers 93% of the solid angle around the collision point. The detector consists of four main components: (a) A 43-layer main drift chamber (MDC) provides momentum measurement for charged tracks with a momentum resolution of 0.5% at 1 GeV/c in a 1 T magnetic field. (b) A time-of-flight system (TOF) composed of plastic scintillators has a time resolution of 80 ps (110 ps) in the barrel (endcaps). (c) An electromagnetic calorimeter (EMC) made of 6240 CsI(Tl) crystals provides an energy resolution for photons of 2.5% (5%) at 1 GeV in the barrel (endcaps). (d) A muon counter (MUC), consisting of 9 (8) layers of resistive plate chambers in the barrel (endcaps) within the return yoke of the magnet, provides 2 cm position resolution. The electron and positron beams collide with an angle of 22 mrad at the interaction point (IP) in order to separate the e^+ and e^- beams after the collision. A GEANT4 [11] based detector simulation package is developed to model the detector response for MC events.

In total, there are 25 data samples taken at different center-of-mass energies or during different periods, as listed in Table I. The data sets are listed chronologically, and the ID number is the requested $E_{\rm cms}$. The offline luminosity is measured through large-angle Bhabha scattering events with a precision of 1% [12]. In this paper, we measure $E_{\rm cms}$ for all the 25 data samples and examine its stability during each data taking period.

III. MUON MOMENTUM VALIDATION WITH J/ψ SIGNAL

The high momentum measurement of muons is validated with $J/\psi \to \mu^+\mu^-$ candidates selected via the process $e^+e^- \to \gamma_{\rm ISR}J/\psi$. Events must have only two good oppositely charged tracks. Each good charged track is required to be consistent with originating from the IP within 1 cm in radial direction ($V_{xy} < 1$ cm) and 10 cm in z direction ($|V_z| < 10$ cm) to the run-dependent IP, and within the polar angle region $|\cos\theta| < 0.8$ (i.e. accepting only tracks in the barrel region). The energy deposition in the EMC (E) for each charged track is required to be less than 0.4 GeV to suppress background from radiative Bhabha events. A further requirement on the opening angle between the two tracks, $\cos\theta_{\mu^+\mu^-} > -0.98$, is used to remove cosmic rays. The background remaining after the above selection comes from the radiative di-muon process, which has exactly the same final state and can not be completely removed. The radiative di-muon events show a smooth distribution in $M(\mu^+\mu^-)$. With the above selection criteria imposed, the distribution of $M(\mu^+\mu^-)$ of each sample is fitted with a crystal-ball function [13] for the J/ψ signal and a linear function to model the background. Figure 1 shows the fit result for the data sample 4600 as an example. In order to reduce the fluctuation of $M(\mu^+\mu^-)$, adjacent data samples with small statistics are combined. Due to final state radiation, $J/\psi \to \mu^+\mu^-\gamma_{\rm FSR}$, the measured $M^{\rm obs}(\mu^+\mu^-)$ is slightly lower than the nominal J/ψ mass [14]. The mass shift due to the FSR photon(s) $\Delta M_{\rm FSR}$ is estimated by simulated samples of the process $e^+e^- \to \gamma_{\rm ISR}J/\psi$ with 50,000 events each, generated at different energies using the generator PHOTOS [15] with FSR turned on and off. The mass shift $\Delta M_{\rm FSR}$ at each $E_{\rm cms}$ is obtained as the difference in $M^{\rm obs}(\mu^+\mu^-)$ between the MC samples with FSR turned on and off. These simulation studies validate that $\Delta M_{\rm FSR}$ is independent of $E_{\rm cms}$. A weighted average, $\overline{\Delta M}_{\rm FSR} = (0.59 \pm 0.04)$ MeV/c^2, is obtained by fitting the $\Delta M_{\rm FSR}$ versus $E_{\rm cms}$. The measured mass corrected by $\overline{\Delta M}_{\rm FSR}$, $M^{\rm cor}(\mu^+\mu^-)$, is plotted in Fig. 2 and listed in Table I (column 4). The values of $M^{\rm cor}(\mu^+\mu^-)$ for the different data samples are consistent within errors, and the average is $\overline{M}^{\rm cor}(\mu^+\mu^-) = 3096.79 \pm 0.08$ MeV/c^2, which agrees with the nominal J/ψ mass within errors. The small difference is considered as systematic uncertainty in Section VII.

IV. THE MASS SHIFT $\Delta M_{\rm ISR/FSR}$

The $E_{\rm cms}$ of the initial e^+e^- pair is measured via the di-muon process $e^+e^- \to \gamma_{\rm ISR/FSR}\mu^+\mu^-$. However, due to the emission of radiative photons, the invariant mass of the $\mu^+\mu^-$ pair is less than the $E_{\rm cms}$ of the initial e^+e^- pair by $\Delta M_{\rm ISR/FSR}$. In general, the mass shift due to the FSR is small, about 0.6 MeV/c^2 at 3.097 GeV, and the mass shift due

TABLE I. Summary of the data sets, including ID, run number, offline luminosity, the measured $M^{\rm cor}(J/\psi)$, $M^{\rm obs}(\mu^+\mu^-)$, and $E_{\rm cms}$. The first uncertainty is statistical, and the second is systematic. Superscripts indicate separate samples acquired at the same $E_{\rm cms}$. The "-" indicates samples which are combined with the previous one(s) to measure $M^{\rm cor}(\mu^+\mu^-)$.

ID	Run number	Offline lum. (pb^{-1})	$M^{\rm cor}(J/\psi)$ (MeV/c^2)	$M^{\rm obs}(\mu^+\mu^-)$ (MeV/c^2)	$E_{\rm cms}$ (MeV)
4009^1	23463 to 23505	481.96±0.01	3097.00±0.15	4005.90±0.15	4009.10±0.15±0.59
4009^2	23510 to 24141		-	4004.26±0.05	4007.46±0.05±0.66
4260^1	29677 to 29805	523.74±0.10	3096.95±0.26	$(4367.37-3.75\times10^{-3}\times N_{\rm run})$ ±0.12	$(4370.95-3.75\times10^{-3}\times N_{\rm run})$ ±0.12±0.62
4260^2	29822 to 30367		-	4254.42±0.06	4258.00±0.06±0.60
4190	30372 to 30437	43.09±0.03	3097.53±0.51	4185.12±0.15	4188.59±0.15±0.68
4230^1	30438 to 30491	44.40±0.03	-	4223.83±0.18	4227.36±0.18±0.63
4310	30492 to 30557	44.90±0.03	-	4304.22±0.17	4307.89±0.17±0.63
4360	30616 to 31279	539.84±0.10	3096.42±0.28	4354.51±0.05	4358.26±0.05±0.62
4390	31281 to 31325	55.18±0.04	3096.39±0.62	4383.60±0.17	4387.40±0.17±0.65
4420^1	31327 to 31390	44.67±0.03	-	4413.10±0.20	4416.95±0.20±0.63
4260^3	31561 to 31981	301.93±0.08	3096.76±0.34	4253.85±0.07	4257.43±0.07±0.66
4210	31983 to 32045	54.55±0.03	3096.88±0.43	4204.23±0.14	4207.73±0.14±0.61
4220	32046 to 32140	54.13±0.03	-	4213.61±0.14	4217.13±0.14±0.67
4245	32141 to 32226	55.59±0.04	-	4238.10±0.12	4241.66±0.12±0.73
4230^2	32239 to 32849	1047.34±0.14	3096.58±0.18	$(4316.81-2.87\times10^{-3}\times N_{\rm run})$ ±0.05	$(4320.34-2.87\times10^{-3}\times N_{\rm run})$ ±0.05±0.60
4230^3	32850 to 33484		-	4222.01±0.05	4225.54±0.05±0.65
3810	33490 to 33556	50.54±0.03	3097.38±0.37	3804.82±0.10	3807.65±0.10±0.58
3900	33572 to 33657	52.61±0.03	-	3893.26±0.11	3896.24±0.11±0.72
4090	33659 to 33719	52.63±0.03	-	4082.15±0.14	4085.45±0.14±0.66
4600	35227 to 36213	566.93±0.11	3096.54±0.33	4595.38±0.07	4599.53±0.07±0.74
4470	36245 to 36393	109.94±0.04	3096.69±0.42	4463.13±0.11	4467.06±0.11±0.73
4530	36398 to 36588	109.98±0.04	-	4523.10±0.11	4527.14±0.11±0.72
4575	36603 to 36699	47.67±0.03	-	4570.39±0.18	4574.50±0.18±0.70
4420^2	36773 to 37854	1028.89±0.13	3096.65±0.21	4411.99±0.04	4415.84±0.04±0.62
4420^3	37855 to 38140		-	4410.21±0.07	4414.06±0.07±0.72

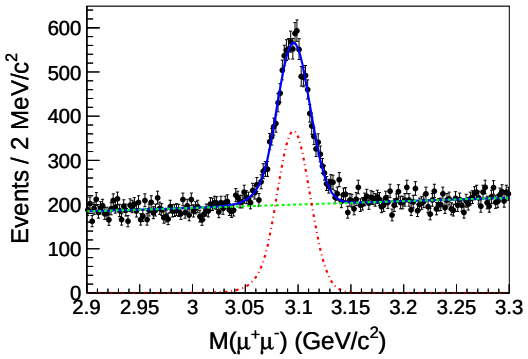

FIG. 1. Fit to the $M(\mu^+\mu^-)$ distribution in $e^+e^- \to \gamma_{\rm ISR}J/\psi$ events for the data sample 4600. Black dots with error bars are data, the blue curve shows the fit result, the red dash-dotted curve is for signal, and the green dashed line is for background.

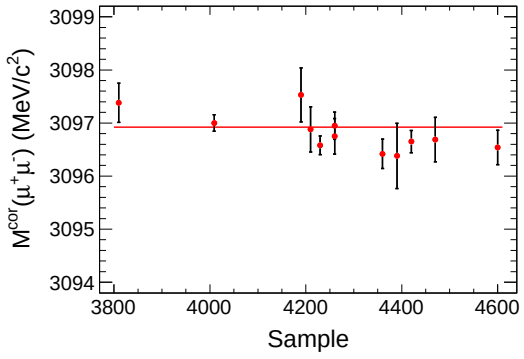

FIG. 2. Measured J/ψ mass after the FSR correction, $M^{\rm cor}(\mu^+\mu^-)$, for data taken at different energies, in which the data samples with small statistics are merged (described in text). The red solid line is the nominal J/ψ mass for reference.

to the ISR is 2∼3 MeV, which has been well studied theoretically [8]. In the analysis, the $\Delta M_{\rm ISR/FSR}$ is estimated with MC simulation using BABAYAGA3.5 [9]. We generate 50,000 di-muon MC events for each sample with ISR/FSR turned on and off, and take the difference in $M(\mu^+\mu^-)$ as the mass shift $\Delta M_{\rm ISR/FSR}$ caused by ISR and FSR. In order to avoid possible bias, the same event selection criteria for the di-muon process applied for data (as described in Section V) are imposed to the MC samples.

The distributions of $M(\mu^+\mu^-)$ with ISR/FSR on and off are fitted with a Gaussian function in a range around the peak (same method with data in Section V). The difference in peak positions (the mass shift $\Delta M_{\rm ISR/FSR}$) versus $E_{\rm cms}$ is seen to increase with $E_{\rm cms}$, as shown in Fig. 3. The $\Delta M_{\rm ISR/FSR}$ is fitted with a linear function, $\overline{\Delta M}_{\rm ISR/FSR} = (-3.53\pm1.11)+(1.67\pm0.28)\times10^{-3}\times E_{\rm cms}/{\rm MeV}$; the good-

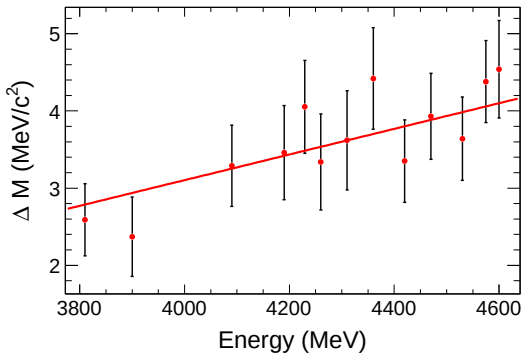

FIG. 3. Difference in $M(\mu^+\mu^-)$ between the MC samples with ISR/FSR turned on and off (the mass shift $\Delta M_{\rm ISR/FSR}$) versus center-of-mass energy for $e^+e^- \to \gamma_{\rm ISR/FSR}\mu^+\mu^-$ MC samples. The red solid line is the fit result.

ness of the fit is $\chi^2/n.d.f = 6.3/13$. The resulting $E_{\rm cms}$-dependent $\overline{\Delta M}_{\rm ISR/FSR}$ will be used to correct the measured $M^{\rm obs}(\mu^+\mu^-)$ for the effects of ISR and FSR.

The mass shift due to FSR only, $\Delta M_{\rm FSR}$, is estimated by comparing MC samples of di-muon production with FSR turned on and off. We find that $\Delta M_{\rm FSR}$ increases with $E_{\rm cms}$ and we parameterize the $E_{\rm cms}$ dependence with a first-order polynomial as $\overline{\Delta M}_{\rm FSR} = (-1.34 \pm 0.84) + (0.56 \pm 0.21) \times 10^{-3} \times E_{\rm cms}$, where $E_{\rm cms}$ is in unit of MeV and the error matrix of the fit parameters is $(0.693, -0.170 \times 10^{-3}, -0.170 \times 10^{-3}, 0.042 \times 10^{-6})$. So the corresponding $\Delta M_{\rm FSR}$ at 3.81 GeV (4.6 GeV) is 0.79±0.09 MeV (1.24±0.14 MeV).

V. THE MEASUREMENT OF $E_{\rm cms}$

To select the di-muon process $e^+e^- \to \gamma_{ISR/FSR}\mu^+\mu^-$, the requirement for charged tracks is the same as the $\gamma_{\rm ISR}J/\psi$ selection. To achieve best precision, only events with both tracks in the barrel region (i.e., in the polar angle region $|\cos\theta| < 0.80$) are accepted. A requirement on the opening angle between the two tracks of $178.60^\circ < \theta_{\mu\mu} < 179.64^\circ$ is applied to suppress cosmic ray and di-muon events with high-energy radiative photons. To further remove cosmic ray events, the TOF timing difference between the two tracks is required to be $|\Delta t| < 4$ ns. The background contribution following above selection criteria is less than 0.001% compared to signal and is therefore neglected in the following.

We estimate the peak position of the distribution of $M^{\rm obs}(\mu^+\mu^-)$ for selected di-muon events by fitting with a Gaussian function in the range of $(-1\sigma, 2\sigma)$ around the peak, where σ is the standard deviation of the Gaussian. To examine the stability of the $E_{\rm cms}$ over time for each data sample, the fit procedure is performed for each run of the data samples, where a run normally corresponds to one hour of data taking. The fit result for one run of the 4600 data sample is shown in Fig. 4. The measured $\mu^+\mu^-$ masses versus the run number for the samples $4009^{1,2}$, $4260^{1,2}$, 4360, $4230^{2,3}$, 4600, and $4420^{2,3}$ are plotted in Fig. 5. For the

TABLE II. Weighted average $E_{\rm cms}$ for all data samples. The first uncertainty is statistical, and the second is systematic.

ID	Weighted average $E_{\rm cms}$ (MeV)
3810	3807.65±0.10±0.58
3900	3896.24±0.11±0.72
4009	4007.62±0.05±0.66
4090	4085.45±0.14±0.66
4190	4188.59±0.15±0.68
4210	4207.73±0.14±0.61
4220	4217.13±0.14±0.67
4230	4226.26±0.04±0.65
4245	4241.66±0.12±0.73
4260	4257.97±0.04±0.66
4310	4307.89±0.17±0.63
4360	4358.26±0.05±0.62
4390	4387.40±0.17±0.65
4420	4415.58±0.04±0.72
4470	4467.06±0.11±0.73
4530	4527.14±0.11±0.72
4575	4574.50±0.18±0.70
4600	4599.53±0.07±0.74

sample 4260^1 (4230^2), the measured $M^{\rm obs}(\mu^+\mu^-)$ changes slowly and is fitted with a linear function. The fit gives $(4367.37\pm53.53)+(-3.75\pm1.80)\times10^{-3}\times N_{\rm run}$ ($(4316.81\pm 7.76) + (-2.87 \pm 0.25) \times 10^{-3} \times N_{\rm run}$) in unit of MeV/$c^2$, where $N_{\rm run}$ is the run number, and the largest value from error propagation is taken as the corresponding statistical uncertainty. For other data samples, $M^{\rm obs}(\mu^+\mu^-)$ remains stable, and the average value is used to calculate $E_{\rm cms}$. The samples 4009^1 (4420^2) and 4009^2 (4420^3) are separated because they show a sudden drop in the average energies. Table I (column 5) summarizes the measured $M^{\rm obs}(\mu^+\mu^-)$ for each sample.

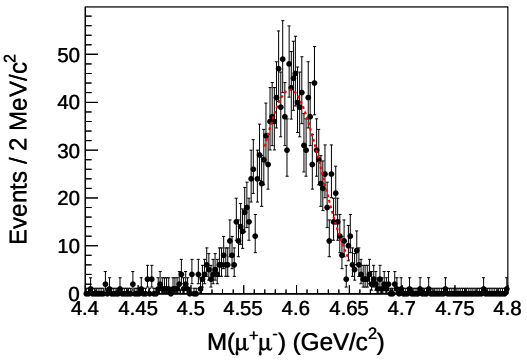

FIG. 4. Fit to the $M(\mu^+\mu^-)$ distribution for the data sample 4600. Black dots with error bars are data, and the red curve shows the fit result.

The $E_{\rm cms}$ is finally obtained by adding the energy-dependent mass shift $\overline{\Delta M}_{\rm ISR/FSR}$ due to ISR/FSR obtained in Section IV to the measured $M^{\rm obs}(\mu^+\mu^-)$. The measured $E_{\rm cms}$ is listed in Table I (column 6); the systematic uncertainty will be discussed in Section VII.

Each of the data sets 4009, 4230, 4260, and 4420 is split into several sub-samples. We calculate the luminosity-

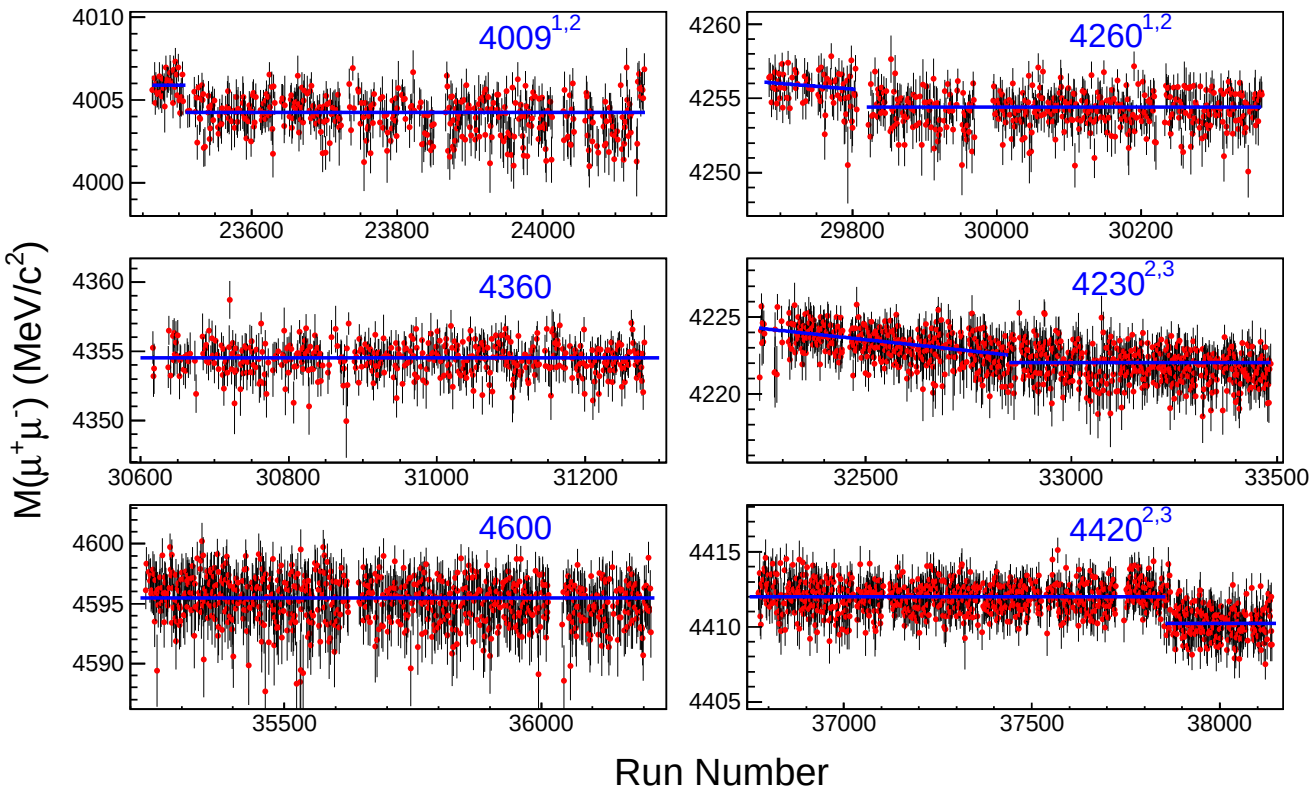

FIG. 5. Measured $M(\mu^+\mu^-)$ of di-muon events run-by-run for samples $4009^{1,2}$, $4260^{1,2}$, 4360, $4230^{2,3}$, 4600, and $4420^{2,3}$. The blue solid lines show the fit results for the data samples.

weighted average $E_{\rm cms}$ for each, and the largest systematic uncertainty of the samples is taken as the systematic uncertainty. In Table II, we summarize the weighted average $E_{\rm cms}$ for all data samples.

VI. CROSS CHECK

The processes of $e^+e^- \to \pi^+\pi^- K^+K^-$ and $e^+e^- \to \pi^+\pi^- p\bar{p}$ are used to check the measurement of the $E_{\rm cms}$. Similar to the di-muon process $e^+e^- \to \gamma_{\rm ISR/FSR}\mu^+\mu^-$, the $E_{\rm cms}$ of the initial e^+e^- system is estimated by the corrected invariant masses of the final state particles $M^{\rm cor}(\pi^+\pi^-K^+K^-)$ and $M^{\rm cor}(\pi^+\pi^-p\bar{p})$. The measurement of the low momentum charged tracks is validated using the decay channels $D^0 \to K^-\pi^+$ and $\bar{D}^0 \to K^+\pi^-$. The measured mass, $M^{\rm obs}(K^-\pi^+/K^+\pi^-) = 1864.00 \pm 0.7$ MeV (statistical uncertainty only) is consistent with the nominal $D^0/\bar{D}^0$ mass [14] with a deviation of 0.84 ± 0.71 MeV. Both the corrected $M^{\rm cor}(\pi^+\pi^-K^+K^-)$ and $M^{\rm cor}(\pi^+\pi^-p\bar{p})$ are found to be consistent with $E_{\rm cms}$ obtained using the di-muon process, with the largest deviation of 0.53 ± 0.75 MeV found in sample 4420.

VII. SYSTEMATIC UNCERTAINTIES

The systematic uncertainty in $E_{\rm cms}$ in this analysis is estimated by considering the uncertainties from the momentum measurement of the $\mu^\pm$, the estimation of the mass shift $\Delta M_{\rm ISR/FSR}$ due to ISR/FSR, the generator, and the corresponding fit procedure.

We use the J/ψ invariant mass via the process $J/\psi \to \mu^+\mu^-$ to check the momentum reconstruction. The measured J/ψ mass corrected for FSR effects at each energy, $M^{\rm cor}(J/\psi)$, is close to the nominal J/ψ mass. To be conservative, we use a first-order polynomial to fit the $M^{\rm cor}(J/\psi)$ versus $E_{\rm cms}$ distribution, and find the largest difference in the J/ψ mass between the fit result and the nominal value to be 0.34 MeV/c^2. We take $\frac{0.34}{3096.92} = 0.011\%$ as the systematic uncertainty due to the momentum measurement.

The mass shift $\Delta M_{\rm ISR/FSR}$ due to ISR/FSR is $E_{\rm cms}$ dependent, and is obtained from MC samples with 50,000 generated events each. The standard deviation of the distribution of $\Delta M_{\rm ISR/FSR}$ versus $E_{\rm cms}$ is given by

$$\sigma = \sqrt{\frac{\Sigma(\Delta M_{\rm ISR/FSR} - \overline{\Delta M}_{\rm ISR/FSR})^2}{N-1}} = 0.37\ {\rm MeV}/c^2, \quad (3)$$

where $\overline{\Delta M}_{\rm ISR/FSR}$ is the value from the fit (Fig. 3), and N is the number of points in Fig. 3. A value of 0.37 MeV/c^2 is

taken as systematic uncertainty due to the ISR/FSR correction.

Additionally, we use different generator versions (BABAYAGA3.5 and BABAYAGA@NLO) to estimate the mass shift $\Delta M_{\rm ISR/FSR}$. The averaged difference in $\Delta M_{\rm ISR/FSR}$ from the two generators is 0.036 ± 0.067 MeV/c^2, which reflects the contribution to the systematic uncertainty of the ISR/FSR correction from the generator; it is negligibly small.

The $M^{\rm obs}(\mu^+\mu^-)$ is measured run-by-run and is found to be stable during data-taking for most samples. For the runs in each sample (except for the samples of 4230^2 and 4260^1, which are described by a first-order polynomial), the average $E_{\rm cms}$ is provided to reduce the statistical fluctuation. If the energy shifts gradually during the data-taking, the simple average value will cause a systematic uncertainty. To estimate this systematic error for each sample, we fit the distribution of $M^{\rm obs}(\mu^+\mu^-)$ versus run-number by a first-order polynomial and take the largest difference between the fitting result and the average value, less than 0.25 MeV on average, as the systematic uncertainty.

The uncertainties from other sources, such as background and event selection, are negligible. Assuming all the sources of systematic uncertainty are independent, the total systematic uncertainty is obtained by adding all items in quadrature, which is listed in Table I (column 6). The uncertainty is smaller than 0.8 MeV for all the data samples.

VIII. SUMMARY

The center-of-mass energies of the data taken from 2011 to 2014 for the studies of the charmonium-like and higher excited charmonium states are measured with the di-muon process $e^+e^- \to \gamma_{\rm ISR/FSR}\mu^+\mu^-$. The corresponding statistical uncertainty is very small, and the systematic uncertainty is found to be less than 0.8 MeV. The measured $E_{\rm cms}$ is validated by the processes $e^+e^- \to \pi^+\pi^- K^+K^-$ and $e^+e^- \to \pi^+\pi^- p\bar{p}$. The stability of $E_{\rm cms}$ over time for the data samples is also examined. For the samples 4009, 4230, 4260, 4420, we also give the luminosity-weighted average $E_{\rm cms}$. The results are essential for the discovery of new states and investigation of the transition of charmonium and charmonium-like states [4–7].

ACKNOWLEDGMENTS

The BESIII collaboration thanks the staff of BEPCII and the IHEP computing center for their strong support. This work is supported in part by National Key Basic Research Program of China under Contract No. 2015CB856700; National Natural Science Foundation of China (NSFC) under Contracts Nos. 11125525, 11235011, 11322544, 11335008, 11425524; the Chinese Academy of Sciences (CAS) Large-Scale Scientific Facility Program; the CAS Center for Excellence in Particle Physics (CCEPP); the Collaborative Innovation Center for Particles and Interactions (CICPI); Joint Large-Scale Scientific Facility Funds of the NSFC and CAS under Contracts Nos. 11179007, U1232201, U1332201; CAS under Contracts Nos. KJCX2-YW-N29, KJCX2-YW-N45; 100 Talents Program of CAS; National 1000 Talents Program of China; INPAC and Shanghai Key Laboratory for Particle Physics and Cosmology; German Research Foundation DFG under Contract No. Collaborative Research Center CRC-1044; Istituto Nazionale di Fisica Nucleare, Italy; Ministry of Development of Turkey under Contract No. DPT2006K-120470; Russian Foundation for Basic Research under Contract No. 14-07-91152; The Swedish Research Council; U. S. Department of Energy under Contracts Nos. DE-FG02-04ER41291, DE-FG02-05ER41374, DE-FG02-94ER40823, DESC0010118; U.S. National Science Foundation; University of Groningen (RuG) and the Helmholtzzentrum fuer Schwerionenforschung GmbH (GSI), Darmstadt; WCU Program of National Research Foundation of Korea under Contract No. R32-2008-000-10155-0.

[1] D. M. Asner *et al.*, Int. J. Mod. Phys. A **24**, 499 (2009).
[2] N. Brambilla *et al.*, Eur. Phys. J. C **71**, 1534 (2011).
[3] E. V. Abakumova *et al.* Nucl. Instrum. Meth. A **659**, 21 (2011).
[4] M. Ablikim *et al.* [BESIII Collaboration], Phys. Rev. Lett. **110**, 252001 (2013).
[5] M. Ablikim *et al.* [BESIII Collaboration], Phys. Rev. Lett. **111**, 242001 (2014).
[6] M. Ablikim *et al.* [BESIII Collaboration], Phys. Rev. Lett. **112**, 022001 (2014).
[7] M. Ablikim *et al.* [BESIII Collaboration], Phys. Rev. Lett. **112**, 132001 (2014).
[8] E. A. Kuraev and V. S. Fadin, Yad. Fiz. **41**, 773 (1985) [Sov. J. Nucl. Phys. **41**, 466 (1985)].
[9] G. Balossini, C. M. Carloni Calame, G. Montagna, O. Nicrosini and F. Piccinini, Nucl. Phys. B **758**, 227 (2006).
[10] M. Ablikim *et al.* [BESIII Collaboration], Nucl. Instrum. Meth. A **614**, 345 (2010).
[11] S. Agostinelli *et al.* [GEANT4 Collaboration], Nucl. Instrum. Meth. A **506**, 250 (2003).
[12] M. Ablikim *et al.* [BESIII Collaboration], Chin. Phys. C **39**, 093001 (2015).
[13] T. Skwarnicki *et al.* [Report No. DESY F31-86-02 1986 (unpublished)].
[14] K. A. Olive *et al.* [Particle Data Group], Chin. Phys. C **38**, 090001 (2014).
[15] E. Barberio and Z. Was, Comput. Phys. Commun. **79**, 291 (1994).